Kinetic Characterization of Novel Pyrazole TGF-β Receptor I Kinase Inhibitors and Their Blockade of the Epithelial−Mesenchymal Transition

Sheng-Bin Peng, Lei Yan, Xiaoling Xia, Scott A. Watkins, Harold B. Brooks, Douglas Beight, David K. Herron, Michael L. Jones, John W. Lampe, William T. McMillen, Nicholas Mort, J. Scott Sawyer, and Jonathan M. Yingling*

Lilly Research Laboratories, Lilly Corporate Center, Indianapolis, Indiana 46285

Received June 3, 2004; Revised Manuscript Received November 8, 2004

ABSTRACT: Transforming growth factor β (TGF-β) signaling pathways regulate a wide variety of cellular processes including cell proliferation, differentiation, extracellular matrix deposition, development, and apoptosis. TGF-β type-I receptor (TβRI) is the major receptor that triggers several signaling events by activating downstream targets such as the Smad proteins. The intracellular kinase domain of TβRI is essential for its function. In this study, we have identified a short phospho-Smad peptide, pSmad3(−3), KVLTQMGSPSIRCSS(PO4)VS as a substrate of TβRI kinase for *in vitro* kinase assays. This peptide is uniquely phosphorylated by TβRI kinase at the C-terminal serine residue, the phosphorylation site of its parent Smad protein *in vivo*. Specificity analysis demonstrated that the peptide is phosphorylated by only TβRI and not TGF-β type-II receptor kinase, indicating that the peptide is a physiologically relevant substrate suitable for kinetic analysis and screening of TβRI kinase inhibitors. Utilizing pSmad3(−3) as a substrate, we have shown that novel pyrazole compounds are potent inhibitors of TβRI kinase with K_i value as low as 15 nM. Kinetic analysis revealed that these pyrazoles act through the ATP-binding site and are typical ATP competitive inhibitors with tight binding kinetics. More importantly, these compounds were shown to inhibit TGF-β-induced Smad2 phosphorylation *in vivo* in NMuMg mammary epithelial cells with potency equivalent to the inhibitory activity in the *in vitro* kinase assay. Cellular selectivity analysis demonstrated that these pyrazoles are capable of inhibiting activin signaling but not bone morphogenic protein or platelet-derived growth factor signal transduction pathways. Further functional analysis revealed that pyrazoles are capable of blocking the TGF-β-induced epithelial−mesenchymal transition in NMuMg cells, a process involved in the progression of cancer, fibrosis, and other human diseases. These pyrazoles provide a foundation for future development of potent and selective TβRI kinase inhibitors to treat human disease.

The transforming growth factor β (TGF-β)[1] superfamily comprises a large number of structurally related polypeptide growth factors. They are important regulators of a wide variety of cellular processes including cell proliferation, differentiation, extracellular matrix deposition, development, and apoptosis (*1*−*4*). The signaling events initiated by these growth factors are mediated through two transmembrane receptors that possess serine/threonine kinase activity (*5*). It has been established that TGF-β, a 25-kDa dimer, binds to the TGF-β type-II receptor (TβRII), which then phosphorylates the TGF-β type-I receptor (TβRI) (*6*, *7*). This phosphorylation event activates TβRI, the major signaling receptor, which can then trigger several signaling pathways by activating downstream targets such as the Smad family of proteins (*8*−*10*). TβRII exists as a constitutively active homodimer in cells and is the primary ligand-binding receptor at the cell surface. In contrast, TβRI is unable to bind ligand in the absence of TβRII and remains inactive until it is recruited into a heteromeric complex along with TβRII following TGF-β binding. This recruitment results in an activating transphosphorylation event within the juxtamembrane-conserved GS domain of TβRI, which then phosphorylates the downstream targets of the signaling pathway. The Smad pathway that was originally discovered in genetic screens of both *Caenorhabditis elegans* and *Drosophila* is the major downstream signaling pathway. Three distinct classes of Smad proteins have been identified: the R-Smads (receptor-activated), the C-Smads (common), and the I-Smads (inhibitory). After TβRI activation, the R-Smads are phosphorylated at their extreme C terminus in the MH2 domain, which results in complex formation with Smad4, the C-Smad, and subsequent nuclear translocation of this heteromeric complex. Once in the nucleus, the Smad complex regulates transcription by two distinct mechanisms that are not mutually exclusive. First, these complexes are capable themselves of directly binding DNA and activating or repressing transcription depending upon the promoter context. Second, Smad complexes can indirectly regulate transcription via their interaction with other transcription

* To whom correspondence should be addressed: Lilly Research Laboratories, Lilly Corporate Center, Indianapolis, IN 46285. Telephone: 317-433-6087. E-mail: yingling_jonathan@lilly.com.

[1] Abbreviations: TGF-β, transforming growth factor β; TβRI, TGF-β type-I receptor; TβRII, TGF-β type-II receptor; Smad, Sma and mothers against decapentaplegic homologue; BMP, bone morphogenic protein; NTA, Ni-nitrilotriacetic acid; TFA, trifluoroacetic acid; EMT, epithelial−mesenchymal transition.

10.1021/bi048851x CCC: $30.25
Published on Web 01/27/2005

factors (e.g., AP1 or SP1) and components of the transcription machinery (e.g., CBP/p300). The I-Smads, Smad6 and Smad7, are homologous to the R-Smads except that they lack the C-terminal sites of phosphorylation and thus act as dominant negatives at the level of receptor and C-Smad interaction.

The role of TGF-β in tumor suppression and tumor promotion has been well-characterized in several model systems (*11*, *12*). Initially, TGF-β is predominantly tumor suppressive, because it potently restricts cell-cycle progression of a number of different cell lineages. However, during the tumorigenic process, this inhibitory pathway is perturbed either by transcriptional deregulation of receptor expression, receptor mutation, or Smad mutation. Although these alterations can completely eliminate TGF-β responses in the tumor cell population, often the ability of TGF-β to regulate certain transcriptional effects in the tumor cells is maintained and contributes to the increased invasive and metastatic potential of the tumor. As tumorigenesis proceeds, TGF-β levels increase in the tumor microenvironment either as a result of secretion from the tumor cells themselves or release from storage depots. The increased levels of TGF-β promote tumorigenesis by stimulating proliferation of mesenchymal cells, inducing immunosuppression, increasing invasive and metastatic potential, enhancing angiogenesis, and increasing the genetic instability of the tumor cells. TGF-β has been implicated in the promotion of breast, prostate, lung, liver, colon, gastric, ovarian, cervical, brain, and skin tumors (*1*−*4*). Therefore, the TGF-β signaling pathway has become an attractive target for oncology drug development.

Epithelial−mesenchymal transition (EMT) was originally described as a normal developmental process (*13*, *14*). In cancer, EMT generally accompanies more aggressive behavior of the tumor cells (*15*, *16*). It was recently reported that inhibition of autocrine TGF-β signaling in carcinoma cells reduces cell invasiveness and tumor metastasis, and these effects of TGF-β are closely associated with its ability to induce EMT and stimulate cell migration (*17*, *18*). TGF-β also plays a central role in tissue fibrogenesis after injury (*19*, *20*). TGF-β-induced EMT again plays an important role in the pathogenic process of chronic renal interstitial fibrosis. Many lines of evidence implicate TGF-β1 as a major pathogenic factor in the initiation and progression of chronic renal interstitial fibrosis, and a characteristic indication of this pathogenic process is the tubular epithelial−myofibroblast transition (*21*). Therefore, TGF-β-induced EMT represents an important morphological and physiological change of the cells involved in the pathogenesis of both cancer and fibrosis.

Specific domains in TβRI and TβRII are important for TGF-β signaling. The extracellular domains of both receptors are required for ligand binding. The cytoplasmic kinase domains of both TβRI and TβRII are involved in dimerization of the receptors, and their catalytic activity is required for TGF-β signaling (*22*, *23*). The kinase domains of TβRI and TβRII contain sequences characteristic of serine/threonine protein kinases. Consistent with this, TβRI has been shown to phosphorylate its primary substrates, Smad proteins, on serine residues (*24*, *25*), whereas TβRII phosphorylates itself and TβRI on serine and threonine residues. Smad protein phosphorylation by activated TβRI is required for TGF-β signaling. Key evidence for a downstream role of TβRI was provided by the examination of a constitutively active form of TβRI kinase (*26*).

Development of TGF-β receptor kinase inhibitors has become an attractive approach for drug development. To date, several selective inhibitors of TβRI kinase have been described (*27*−*32*). Several pharmaceutical and biotechnology companies are actively pursuing efforts to identify potent and selective TβRI kinase inhibitors for clinical development. However, there is no identified peptide substrate that is suitable for *in vitro* kinase assays and compound screening. In this study, we have designed a set of short peptides based upon the C-terminal sequence of R-Smads, Smad2 and Smad3, and identified that phospho-Smad2 or -Smad3 peptides at the −3 serine residue are specific and physiologically relevant substrates for TβRI kinase. These substrates are suitable for kinetic analysis and high throughput screening of TβRI kinase inhibitors. In addition, we have demonstrated that some novel pyrazole compounds are potent inhibitors of TβRI kinase with K_i values as low as 15 nM. Kinetic analysis revealed that these pyrazoles are ATP competitive inhibitors with tight binding kinetics. These compounds inhibit TGF-β-induced Smad2 phosphorylation *in vivo* in NMuMg mammary epithelial cells with potency equivalent to the inhibitory activity in *in vitro* kinase assays. Cellular selectivity analysis demonstrated the highly selective nature of this chemical scaffold even within the TGF-β superfamily (e.g., BMP signaling) and confirmed previous reports of activin-signaling cross-reactivity (*27*−*29*). Functional analysis revealed that these compounds are capable of blocking TGF-β-induced EMT in NMuMg cells. Therefore, this class of pyrazoles provides a promising chemical foundation for further drug development.

EXPERIMENTAL PROCEDURES

Materials. NMuMg mammary epithelial cells and HeLa cells were obtained from ATCC. Recombinant human TGF-β1 was from R and D Systems. Chemicals for SDS−PAGE were purchased from Invitrogen. Ni-nitrilotriacetic acid (NTA) agarose for protein purification was from Qiagen. Trifluoroacetic acid (TFA), ethylenediaminetetraacetic acid (EDTA), phosphoric acid, and acetonitrile were purchased from Fisher Scientific. All HPLC column measurements were performed on a Hewlett−Packard 1100 system using C18 reversed phase. [γ-^{32}P]ATP (2200 Ci/mmol, 170 TBq/mmol) and [γ-^{33}P]ATP (3000 Ci/mmol, 111TBq/mmol) were from Perkin−Elmer. MultiScreen-MAPH and MAFB filter plates for filter-binding assays were from Millipore. Phalloidin-Alexa 488, the E-cadherin antibody, and anti-rabbit IgG conjugated with Alexa 488 were obtained from Molecular Probes. P-p38, P-ATF2, P-MAPKAP2, P-JNK, p38 antibodies for Western blotting were obtained from Cell Signaling.

TβRI Kinase Domain Expression and Purification. The intracellular kinase domain of TβRI (ALK5) and its constitutively active mutation, T204D, were cloned and expressed in Sf9 insect cells by standard procedures as described (*30*). The proteins were purified from Sf9 cells on a single Ni-NTA-affinity column. Briefly, Sf9 cells expressing the TβRI kinase domain or its constitutively active mutation, T204D, were harvested and lysed in buffer consisting of 50 mM Tris-HCl at pH 7.5, 150 mM NaCl, 50 mM NaF, 0.5% NP-40, 20 mM β-mercaptoethenol, 10 mM imidazole, 1 mM PMSF,

and 1× EDTA-free protease inhibitor cocktail (Roche). After centrifugation, the lysate was loaded onto a Ni-NTA column and the protein was eluted with a linear 0−200 mM imidazole gradient prepared in kinase buffer containing 50 mM Tris-HCl, 150 mM NaCl, 4 mM $MgCl_2$, 1 mM NaF, and 2 mM β-mercaptoethenol. The purity of the purified kinase was analyzed by SDS−PAGE, and selected fractions were pooled and utilized for kinase assays.

Peptide-Substrate Design and Synthesis. Peptides with 17 or 18 residues were designed and synthesized based upon the carboxyl-terminal sequences of Smad2 and Smad3 proteins. Because Smad2 and Smad3 are phosphorylated by TβRI at the extreme C-terminal serine residues (−1 and −3 positions) under physiological conditions, phosphoserine was incorporated into the −1 or −3 position of some synthesized peptides. In addition, one or two lysines were added at the N terminus of each peptide to facilitate peptide binding to the MultiScreen-MAPH filter (a phosphocellulose and negatively charged filter paper) in the filter-binding assay. These peptides were synthesized by AnaSpec, Inc., and the final products were purified via reverse-phase HPLC. The identity of each peptide was confirmed by electrospray mass spectrometry. The synthesized peptides tested in this study are Smad2, KVLTQMGSPSVRCSSMS; pSmad2(−1), KVLTQMGSPSVRCSSMpS; pSmad2(−3), KVLTQMGSPSVRCSpSMS; pSmad3(−1), KVLTQMGSPSIRCSSVpS; pSmad3(−3), KVLTQMGSPSIRCSpSVS; pKSmad3(−3), KKVLTQMGSPSIRCSpSVS; pKSmad3(−1, −3), KKVLTQMGSPSIRCSpSVpS; and pKSmad3(Ala, −3), KKVLTQMGSPSIRCSpSVA.

Gel-Based Peptide-Substrate Phosphorylation Assay. Reaction mixtures (40 μL), containing 50 mM HEPES at pH 7.5, 1 mM NaF, 10 mM $MgCl_2$, 8 μM ATP, 1 μCi [γ-^{32}P]-ATP (2200 Ci/mmol), 100 μM peptide substrate, and 100 nM TβRI kinase or the T204D mutant were incubated at 30 °C for 30 min. The reactions were terminated by the addition of an equal volume of 2× SDS−PAGE sample buffer. A total of 20 μL of the mixture was then loaded on a 10−20% SDS−polyacrylamide-gradient gel. After electrophoresis, the gel was fixed with 50% methanol and 15% acetic acid, dried by a GelAir Dryer from Bio-Rad, and exposed to X-ray film overnight or a phosphoimaging screen for 1−2 h. Quantitation was performed with a phosphoimager (Molecular Imager FX) and Quantity One software from Bio-Rad.

HPLC−Mass Spectrum Analysis of Peptide Substrate pSmad3(−3) and Its Phosphorylated Product. Typically, reactions were performed in a 40 μL reaction mixture containing 50 mM HEPES at pH 7.5, 1 mM NaF, 5 mM $MgCl_2$, 8 μM ATP, 100 μM peptide substrate pSmad3(−3), and 100 nM TβRI T204D. The reactions were incubated for 60 min at 30 °C and terminated by the addition of 100 mM EDTA. The reaction mixtures were analyzed by HPLC using a Hewlett−Packard Series 1100 system equipped with an autosampler. The reaction mixtures (20 μL) were injected into a reversed-phase column (Vydac C18), and the substrate and its phosphorylated product were separated using a 15−35% linear acetonitrile gradient in 0.1% TFA with a flow rate 1 mL/min. Peak detection was accomplished by monitoring the absorbance at 214 nm, and the molecular mass of each peak was detected by electrospray mass spectrometry.

Filter-Binding Assay. Reactions were performed in a polypropylene 96-well U-bottom microtiter plate. Reactions (40 μL) containing 50 mM HEPES at pH 7.5, 1 mM NaF, 10 mM $MgCl_2$, and different concentrations of ATP, pKSmad3(−3), TβRI kinase, and inhibitors were incubated for 30 min at 30 °C. The reactions were terminated by the addition of 100 μL of 0.5% phosphoric acid. The mixtures were then transferred to a 96-well MultiScreen-MAPH filter plate, which was pre-equilibrated with 0.5% phosphoric acid for 30 min and incubated for 30 min at room temperature. The plate was then washed 3 times by filtration with 300 μL of 0.5% phosphoric acid with a vacuum filtration apparatus from Millipore. After washing, the filter plate was transferred to a MultiScreen Adaptor plate (Perkin−Elmer), 100 μL of Microscint 20 was added to each well, and the radioactivity was determined on a Microplate Scintillation Counter from Packard.

K_m Determination. The K_m values for ATP and peptide substrates were determined by a gel-based assay as described above. To measure the K_m of ATP, reactions containing 50 mM HEPES at pH 7.5, 1 mM NaF, 10 mM $MgCl_2$, 400 μM pSmad3(−3), 100 nM TβRI kinase or the T204D mutant, and a dilution series of ATP from 0 to 500 μM were incubated for 30 min at 30 °C and terminated by the addition of an equal volume of SDS−sample buffer. To measure the K_m values of peptide substrates, reactions containing 50 mM HEPES at pH 7.5, 1 mM NaF, 10 mM $MgCl_2$, 100 μM ATP, 100 nM of the T204D mutant, and a dilution series of peptide substrate from 0 to 1000 μM were incubated for 30 min at 30 °C and terminated by the addition of SDS−sample buffer. The reaction mixtures (20 μL) were then loaded onto a 10−20% SDS−polyacrylamide-gradient gel. After electrophoresis, gels were fixed by 50% methanol and 15% acetic acid and dried with a GelAir Dryer from Bio-Rad. After exposure to a phosphoimager for 1−2 h, the radioactive bands were analyzed by a phosphoimager equipped with Quantity One software from Bio-Rad. The K_m was calculated in SigmaPlot using the enzyme kinetics module.

Determination of Substrate Specificity of pSmad3(−3). To determine the specificity of peptide substrate pSmad3(−3), we investigated if TβRII was able to catalyze the phosphorylation of this peptide substrate. The kinase domain of TβRII was expressed and purified from Sf9 cells with one step Ni-NTA-affinity column (Yingling et al., unpublished data). The gel-based assay as described above was utilized for this specificity determination. Briefly, 40 μL reaction mixtures, containing 50 mM HEPES at pH 7.5, 1 mM NaF, 10 mM $MgCl_2$, 8 μM ATP 1 μCi [γ-^{32}P]ATP (2200 Ci/mmol), 100 μM peptide substrate, and 100 nM TβRI kinase or different concentrations of TβRII kinase, were incubated at 30 °C for 30 min. The autophosphorylation and peptide-substrate phosphorylation were visualized by SDS−PAGE and autoradiography.

K_i Determination and Mechanism of Action Studies. K_i values and mechanism of action of selected pyrazoles were determined by the filter-binding assay. In a 96-well microtiter plate, an appropriate titration of the inhibitor, ATP, and substrate pSmad3(−3) was utilized. A 6-point titration was generally utilized with the inhibitor, ATP, and the peptide substrate. The titration used for each inhibitor varied depending upon the potency of the compound. To analyze if the compound competed with ATP, an ATP titration with

concentrations of 0, 6.25, 12.5, 25, 50, and 100 μM ATP was used and the substrate pKSmad3(−3) and T204D mutant enzyme were fixed at 200 μM and 100 nM, respectively. To analyze if an inhibitor competed with substrate pKSmad3(−3), a pKSmad3(−3) titration with concentrations of 0, 50, 100, 200, 400 and 800 μM was used and ATP and T204D mutant were fixed at 25 μM and 100 nM, respectively. The reactions were incubated for 30 min at 30 °C and terminated by the addition of 0.5% phosphoric acid. The K_i and competitive mechanism of each inhibitor were determined by kinetic analyses with Mathematica (version 4.1) software from Microsoft.

Kinetic Binding Type Determination of Selected Pyrazoles. To determine the kinetic binding type of pyrazole inhibitors, we first performed an enzyme titration experiment with constitutively active enzyme, TβRI T204D. Briefly, 40 μL reactions containing a dilution series of the T204D mutant at concentrations of 800, 600, 400, 300, 200, 150, 100, 75, 50, 37.5, 25, and 0 nM in 50 mM HEPES at pH 7.5, 1 mM NaF, 200 μM pKSmad3(−3), and 50 μM ATP were incubated at 30 °C for 30 min. The linear reaction range of enzyme was determined by a linear regression analysis. The IC_{50} of LY364947 and LY566578 at different enzyme concentrations were determined by the filter-binding assay. Typically, 40 μL reactions in 50 mM HEPES at pH 7.5, 1 mM NaF, 200 μM pKSmad3(−3), and 50 mM ATP containing a titration of each inhibitor with concentrations of 1600, 800, 400, 200, 100, 50, 25, and 0 nM were incubated at 30 °C for 30 min. The IC_{50} was calculated using a nonlinear regression method with GraphPad Prism software. The binding type was determined by plotting the correlation between enzyme concentrations and IC_{50} values.

Autophosphorylation of TβRI Kinase and IC_{50} Determination. Autophosphorylation of TβRI kinase was performed as described (*30*). Briefly, 200 nM constitutively active RI T204D enzyme was incubated for 60 min at 30 °C in kinase buffer containing 50 mM Tris-HCl at pH 7.5, 150 mM NaCl, 4 mM $MgCl_2$, 1 mM NaF, 2 mM β-mercaptoethanol, 4 μM ATP, and 1 μCi [γ-^{33}P]ATP. Reactions were terminated by the addition of 25% TCA, and BSA was then added to a final concentration of 250 μg/mL. The autophosphorylated TβRI kinase was captured on MultiScreen-MAFB filter (pure borosilicate glass fiber) plates. The radioactivity was determined on a Microbeta JET Trilux counter from Wallac. For IC_{50} determination, a 10-point titration with a 1:2 dilution for each compound was selected. The IC_{50} is calculated using a nonlinear regression method with GraphPad Prism software.

Western Blot Analysis of in Vivo Phospho-Smad2 in NMuMg Cells. Western blot analysis of phospho-Smad2 protein in NMuMg mammary epithelial cells was performed by standard protocol. Briefly, 2×10^6 NMuMg cells were grown overnight on a 100 mm plate in DMEM with 10% FBS and then starved for 1 h by switching to DMEM containing 0.5% FBS and a dilution series of LY364947 (10 μM, 1:2 dilutions) or LY580276 (20 μM, 1:3 dilutions). Cells were then treated with 2.5 ng/mL (100 pM) TGF-β1 and incubated for 2 h at 37 °C. The cells were washed with 1× PBS and lysed in 150 μL lysis buffer containing 50 mM Tris-HCl at pH 7.5, 500 mM NaCl, 1% NP-40, 0.25% Na-deoxycholate, 20 mM NaF, protease inhibitor cocktail (Roche), and phosphatase inhibitor cocktail I and II (Sigma). A total of 50 μg of protein was loaded onto a 10% SDS−polyacrylamide gel. Western blot analysis was performed with the PS2 phospho-Smad2 antibody.

Cellular Pathway Selectivity Analysis. The TGF-β growth inhibition assay in NMuMg cells was performed as described previously for mink lung epithelial cells (*30*). The xVent2-luciferase BMP4 reporter assay in NMuMg cells was performed as follows. A stable clone harboring the xVent2-lux plasmid was seeded at 1.2×10^4 cells per well in 96-well microtiter plates and allowed to adhere overnight. Cells were serum-starved in 0.5% FBS media containing a dilution series of inhibitor for 2 h prior to the addition of 500 pM BMP4. Luciferase activity was determined 24 h later as previously described (*30*). Western blot analysis of MAP kinases and their downstream effectors in HeLa cells was performed as follows. A total of 2.5×10^5 cells were seeded in 6-well plates in 1 mL of RPMI1640 containing 10% FBS and allowed to adhere overnight. Cells were treated with a dilution series of compound for 1 h prior to the addition of 10 ng/mL TNFα for 15 min. The cells were then washed with ice-cold PBS and lysed in 100 μL of lysis buffer. A total of 10 μg of cell lysate was loaded onto a 4−20% SDS−polyacrylamide gel, and Western blot analysis was performed according to standard protocols.

TGF-β-Induced EMT and Immunofluorescence Microscopy. NMuMg cells were plated at a density of 1×10^4 cells in 10% FBS DMEM on chamber coverglass and allowed to adhere overnight. TGF-β1 (100 pM) was added for an additional 24 h prior to fixation in 1% formaldehyde prepared in 1× PBS for 10 min at room temperature. Fixed cells were washed twice for 10 min each with 1× PBS and then permeabilized in 1× PBS plus 1% BSA and 0.025% NP-40 for 15 min at room temperature. After permeabilization, cells were washed twice with 1× PBS and 1% BSA and then incubated for 30 min at room temperature with protein-blocker buffer (Dako). Phalloidin-Alexa 488 at 1:26 dilution and anti-E-cadherin at 1:75 dilution were added and incubated for 1 h in a dark humid chamber. After the primary incubation, the cells were again washed with 1× PBS and 1% BSA 3 times and the E-cadherin samples were then incubated for 1 h with anti-rabbit IgG conjugated with Alexa 488 at a 1:500 dilution. After washing with 1× PBS and 1% BSA, the cells were counter-stained with propidium iodide at a 1:20 dilution. After a final wash with 1× PBS, the cells were visualized by confocal microscopy.

RESULTS

Phosphorylation of Synthesized Peptides by TβRI Kinase. To identify a short peptide substrate suitable for TβRI kinase, we have synthesized a set of peptides based upon the carboxyl sequences of Smad2 and Smad3 proteins as listed in the Experimental Procedures. The purity and identity of each synthetic peptide was confirmed by HPLC and mass spectrum analysis (data not shown). Subsequently, 5 peptides, Smad2, pSmad2(−1), pSmad2(−3), pSmad3(−1), and pSmad3(−3), were tested for phosphorylation by TβRI T204D kinase in a gel-based assay as described in the Experimental Procedures. As demonstrated in Figure 1A, all five peptides were phosphorylated by TβRI T204D kinase. Interestingly, phospho-Smad peptides are better substrates

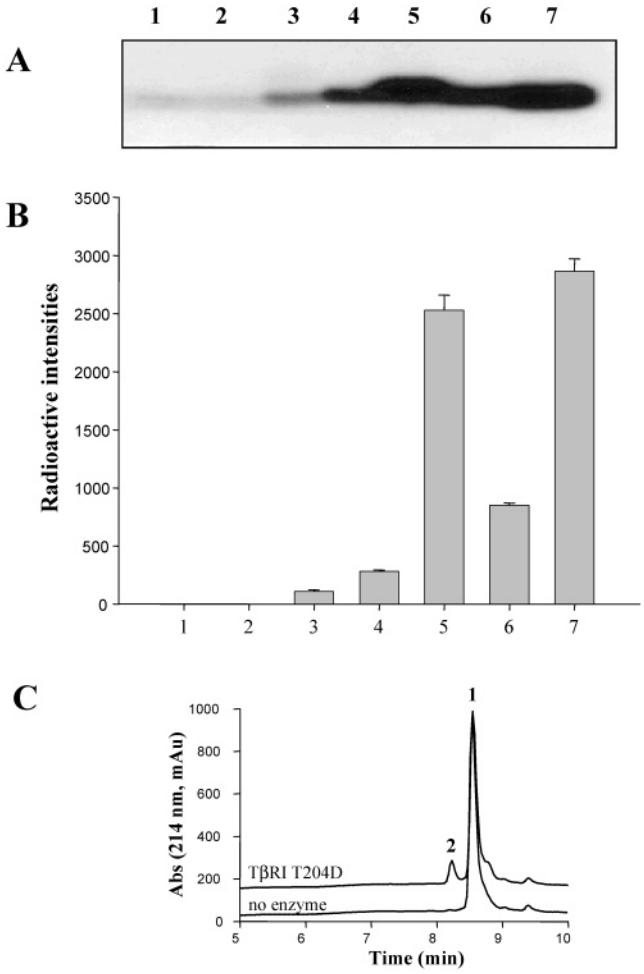

FIGURE 1: Phosphorylation of synthetic peptides by TβRI kinase. (A) SDS−PAGE of synthetic Smad peptide phosphorylation by TβRI kinase. (B) Phosphoimager and densitometric analysis of phosphorylated Smad peptides. Lane or column 1, no enzyme control; lane 2, no peptide-substrate control; lane 3, peptide Smad2; lane 4, pSmad2(−1); lane 5, pSmad2(−3); lane 6, pSmad3(−1); and lane 7, pSmad3(−3). (C) HPLC analysis of pSmad3(−3) peptide substrate (peak 1) in the absence (lower tracing) or presence (upper tracing) of 100 nM TβRI T204D kinase. Electrospray mass spectrum analysis confirmed the addition of a single phosphate group in the product peak (peak 2).

than the nonphospho-Smad2 peptide, with pSmad3(−3) (lane 7) and pSmad2(−3) (lane 5) showing the highest level of phosphorylation. pSmad2(−1) (lane 4) and pSmad3(−1) (lane 6) are modestly phosphorylated, and the native Smad2 peptide is poorly phosphorylated (lane 3). Further densitometric analysis shows that pSmad3(−3) and pSmad2(−3) as substrates of TβRI kinase are at least 50-fold better than the native, nonphospho-Smad2 peptide and 5−10-fold better than pSmad2(−1) or pSmad3(−1) (Figure 1B). Clearly, the phosphoserine at −3 position of either pSmad3(−3) or pSmad2(−3) greatly improved the efficiency of phosphorylation. Overall, pSmad3(−3) showed the best activity and was chosen for further characterization and assay development. It should be noted that the results in Figure 1 were obtained with the TβRI T204D mutant, however, similar results were obtained with wild-type TβRI kinase (data not shown).

HPLC−Mass Spectrum Analysis of Substrate pSmad3(−3) and Its Product. To further characterize pSmad3(−3) as a substrate of TβRI kinase, we have performed an HPLC−mass spectrum analysis of pSmad3(−3) and its phosphorylated product. Peptide pSmad3(−3) showed one major peak with a retention time of 8.6 min in the HPLC profile (peak 1 of Figure 1C). After incubation with TβRI T204D kinase, an additional peak with a retention time of 8.2 min appeared (peak 2 of Figure 1C). The substrate and product peaks were well-separated by reverse-phase HPLC with a 15−35% acetonitrile gradient. The identities of both peaks were confirmed by mass spectrum analysis. The substrate peak (peak 1) had a molecular mass of 1861, equal to its theoretical mass, and the product peak (peak 2) had a molecular mass of 1941. The difference of molecular masses between the substrate and the product is exactly 80, consistent with the theoretical mass of a single phosphate group. These data suggest that only one phosphate group was added to the pSmad3(−3) peptide after incubation with TβRI T204D kinase, although there are multiple potential phosphorylation sites in this peptide.

Phosphorylation of pSmad3(−3) Occurs Specifically at the −1 Serine Residue. Smad2 and Smad3 proteins are physiologic substrates of TβRI within cells. The extreme carboxy-terminal serines at positions −1 and −3 are specifically phosphorylated *in vivo* by TβRI (*24*, *25*). The synthetic peptide substrate pSmad3(−3) contains four nonphosphorylated serines and one nonphosphorylated threonine, and all are potential phosphorylation sites under *in vitro* conditions. Although the phosphorylation of pSmad3(−3) by TβRI T204D kinase occurred at only one site, the exact phosphorylation site cannot be determined by mass spectrum analysis. To confirm that the phosphorylation of pSmad3(−3) specifically occurred at the −1 serine residue similar to its parental Smad3 protein *in vivo*, we synthesized three peptides: pKSmad3(−3), a peptide identical to pSmad3(−3) with one additional lysine in the N terminus to enhance its binding to the phosphocellulose filter in the filter-binding assay, pKSmad3(−1, −3), and pKSmad3(Ala, −3), where the C-terminal serine residue at the −1 position was either synthetically phosphorylated or replaced by an alanine, respectively. Upon incubation with either wild-type TβRI kinase or the T204D mutant, no phosphorylation was observed on the pKSmad3(−1, −3) or pKSmad3(Ala, −3) (lanes 2 and 3 of parts A and B of Figure 2), while pKSmad3(−3) was efficiently phosphorylated under the same assay conditions (lane 1 of parts A and B of Figure 2). These results confirmed that the phosphorylation of pKSmad3(−3) by TβRI kinase uniquely occurred at the −1 serine residue, the same residue phosphorylated *in vivo* by TβRI. Thus, the pKSmad3(−3) peptide is a physiologically relevant substrate of TβRI kinase and is ideally suited for the identification of TβRI kinase inhibitors. It should be pointed out that peptide pKSmad3(−3) was phosphorylated as efficiently as pSmad3(−3) in a side by side comparison experiment (data not shown). The addition of a lysine to the peptide is to enhance binding to the phosphocellulose filter in the filter-binding assay. Indeed, pKSmad3(−3) bound to the MultiScreen-MAHP filter approximately 2-fold better than pSmad3(−3). Importantly, the addition of this lysine to the substrate did not change its kinetic properties. The constant K_m of pSmad3(−3) and pKSmad3(−3) is virtually the same as shown below.

TGF-β Receptor Specificity of pSmad2(−3) and pSmad3(−3). To evaluate the specificity of pSmad3(−3) and

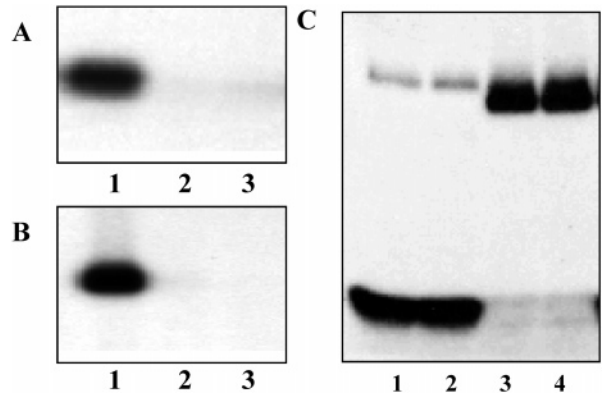

FIGURE 2: Identification of the peptide phosphorylation site and TGF-β receptor specificity. Three peptides, pKSmad3(−3) (lane 1), pKSma3(−1, −3) (lane 2), and pSmad3(Ala, −3) (lane 3) were incubated with either the wild type (A) or constitutively active mutant T204D (B) of TβRI kinase. (C) TGF-β receptor specificity. TβRI wild type (lanes 1 and 2), TβRII (lanes 3 and 4), and peptides pSmad2(−3) (lanes 1 and 3) or pSmad3(−3) (lanes 2 and 4). Upper bands are autophosphorylated receptor kinases, and lower bands are the phosphopeptides.

pSmad2(−3) as TβRI kinase substrates, we investigated if TβRII kinase is able to phosphorylate these peptides. For this purpose, we have cloned the kinase domain of TβRII and purified the kinase to homogeneity with a similar protocol to that of TβRI kinase (Yingling et al., unpublished data). TβRI and TβRII belong to the same family of receptor serine/threonine kinases. The kinase domains of both receptors are highly conserved and share approximately 40% identity. As demonstrated in Figure 2C, the TβRII kinase was able to autophosphorylate effectively under these assay conditions, demonstrating that the purified TβRII kinase is active. However, it was unable to phosphorylate pSmad2(−3) (lane 3 of Figure 2C) or pSmad3(−3) (lane 4 of Figure 2C), whereas the TβRI kinase phosphorylated both peptides effectively (lanes 1 and 2 of Figure 2C). We utilized different concentrations of TβRII kinase and a variety of assay conditions to test if TβRII could phosphorylate these peptides. Under all experimental conditions tested, no phosphorylation was observed (data not shown). These results indicate that peptides pSmad3(−3) and pSmad2(−3) are specific substrates for TβR1 and not its close family member, TβRII. This observation is consistent with the substrate specificity within cells, where Smad proteins are specifically phosphorylated by the TβRI kinase and not TβRII.

K_m Determination of ATP and Peptide Substrates. The Michaelis−Menten term (K_m) for ATP was measured with both wild-type TβRI kinase and the T204D mutant by a gel-based assay utilizing pSmad3(−3) as the substrate. The K_m values of ATP for wild-type kinase and constitutively active mutant T204D were 8.8 and 5.7 μM, respectively, as calculated by nonlinear regression analysis. Additionally, the K_m values for peptide substrates pSmad3(−3) and pSmad2(−3) were also determined using the T204D mutant. The calculated K_m values for pSmad3(−3) and pSmad2(−3) were 260.3 and 331.3 μM, respectively. It appears that pSmad3(−3) is a slightly better substrate than pSmad2(−3) for TβRI kinase. In addition, the K_m for pKSmad3(−3), the peptide designed for the filter-binding assay, was determined to be 288.8 μM, virtually identical to the K_m value 260.3 μM of pSmad3(−3). The addition of a lysine to the N terminus of the peptide did not change the affinity of the peptide.

Table 1: K_i and Mechanism of Action of Selected Pyrazole Inhibitors

Compounds	Structure	K_i (μM)	IC_{50} (μM)[a]	Competition type	
				ATP	substrate
LY364947		0.028[b]	0.580[b]	Yes	No
LY566578		0.038[b]	0.070[b]	Yes	No
LY580276		0.037[b]	0.175[b]	Yes	No
1		0.476	0.555[b]	Yes	No
2	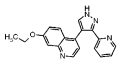	0.024	0.030[b]	Yes	No
3	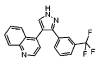	0.128	0.217[b]	Yes	No
4		0.245	0.275[b]	Yes	No
5		0.015[b]	0.031[b]	Yes	No

[a] Measured by autophosphorylation of T204D. [b] Average of multiple measurements with pSmad3(−3) as the substrate.

Pyrazoles Are Potent and ATP Competitive Inhibitors. The identification of peptide pSmad3(−3) as a substrate of TβRI kinase provides a powerful tool for kinetic studies of TβRI kinase and its inhibitors. We have utilized this peptide to measure K_i values and perform mechanism of action studies for select novel pyrazole inhibitors characterized previously in an autophosphorylation assay (*30*). As summarized in Table 1, these pyrazoles are generally potent inhibitors with K_i values as low as 15 nM. All eight compounds analyzed are competitive with ATP but not with the peptide substrate. Figure 3 is an example of the kinetic plots obtained with compound LY364947. The K_i apparent of the compound increased linearly with increasing ATP concentration, a pattern typical of a competitive mechanism (Figure 3A). However, the K_i apparent remained similar when increasing the substrate concentration, characteristic of noncompetitive inhibition (Figure 3B). The same competitive mechanism was observed with the other pyrazole compounds analyzed (Table 1). Interestingly, compound potency in the original autophosphorylation assay is highly correlated with the K_i values determined in the pSmad3(−3) peptide-substrate assay (Figure 3C). The kinetic characterization of these pyrazole compounds as ATP competitive inhibitors is consistent with the ATP-binding site interactions observed by X-ray crystallography for this series (*30*, *31*). This kinetic property in conjunction with the structural information from X-ray crystallography is important for further studies of structure−activity relationships to improve the potency and selectivity of these compounds. Indeed, the 4-phenyl-substituted pyrazoles (e.g., LY580276 and LY566578) are highly selective for TβRI, having a >100-fold decreased activity against TβRII and a >200-fold selectivity against a panel of 40 other

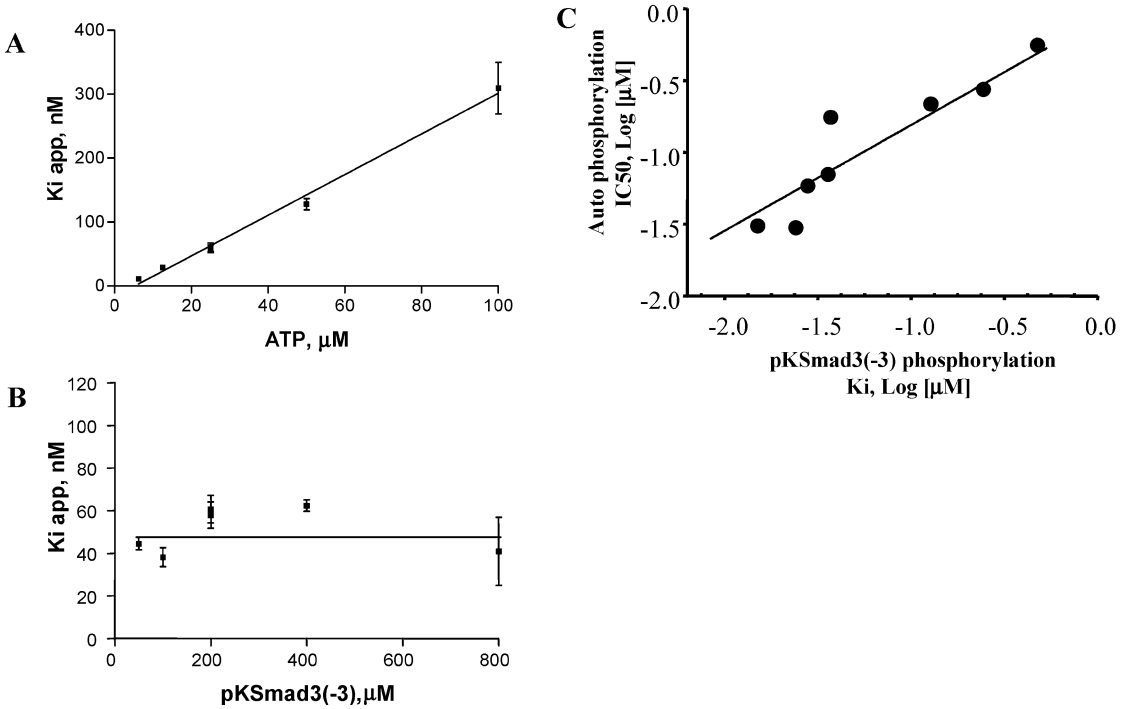

FIGURE 3: Mechanism of action and correlation with autophosphorylation for the pyrazole inhibitors of TβRI kinase. (A) Kinetic profile of ATP titration with LY364947. (B) Kinetic profile of peptide-substrate titration with LY364947. (C) Correlation of autophosphorylation potency (IC_{50}) with K_i as determined in the P-Smad3(−3) substrate assay. The K_i value of the eight pyrazoles shown in Table 1 was determined with the TβRI T204D enzyme and pKSmad3(−3) as the substrate. The IC_{50} value of these same compounds was also determined by autophosphorylation of TβRI T204D. This analysis shows a correlation ($R = 0.75$) between K_i values measured with substrate phosphorylation and IC_{50} values obtained with autophosphorylation.

kinases including AKT, p38, ERK, JNK, MEK1, MKK4, MKK6, MKK7, GSK3β, PKC, c-RAF, c-SRC, and p70S6K.

Pyrazoles Are Tight-Binding Inhibitors. To further characterize the kinetic properties of these pyrazoles with the identified substrate and established assay, we were interested in determining if these pyrazoles are tight- or nontight-binding inhibitors. A tight-binding inhibitor is characterized by the property that the formation of the enzyme−inhibitor complex significantly depletes the availability of the inhibitor. To precisely define this binding property for pyrazole inhibitors, we first determined the linear reaction range of the T204D mutant enzyme. As demonstrated in Figure 4A, the enzyme titration showed that the kinase activity with pKSmad3(−3) as substrate was linear from 100 to 400 nM of T204D. Subsequently, two compounds, LY364947 and LY566578, were selected for binding-type studies. As depicted in Figure 4B, the IC_{50} values of both compounds increased linearly with increasing enzyme concentration, a typical kinetic pattern for a tight-binding inhibitor. Therefore, these potent pyrazoles are tight-binding inhibitors.

Pyrazoles Selectively Inhibit TGF-β-Induced Smad2 Phosphorylation in Vivo in NMuMg Cells. We have demonstrated that the pyrazole inhibitors inhibit peptide-substrate phosphorylation catalyzed by the intracellular kinase domain of TβRI. To explore whether these compounds inhibit the kinase activity of TβRI *in vivo*, we investigated the ability of these compounds to inhibit the phosphorylation of the physiological substrates of TβRI within mammary cells by Western blot analysis. Phospho-Smad2 was not detectable in NMuMg cells in the absence of TGF-β treatment (lane 1 of parts A and B of Figure 5). After activation with recombinant human TGF-β1, phospho-Smad2 was greatly increased (lane 2 of parts A and B of Figure 5). Selected pyrazole inhibitors

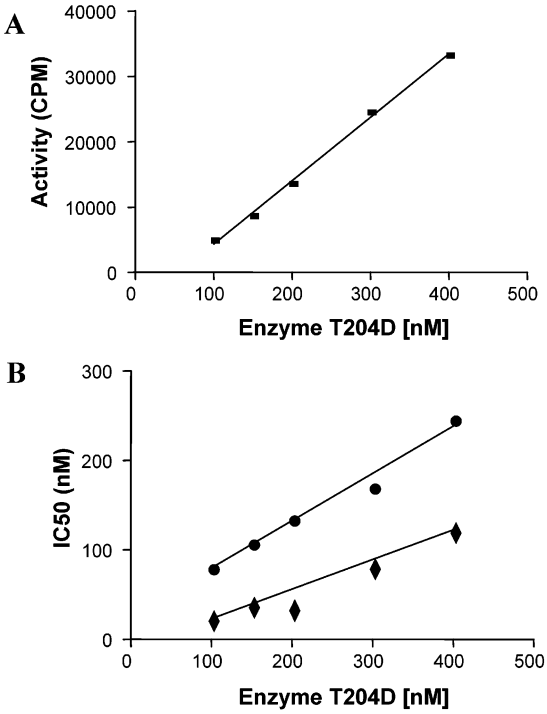

FIGURE 4: Determination of the tight- or nontight-binding mode of pyrazole inhibitors. (A) Enzyme concentration titration of TβRI T204D kinase in the pSmad3(−3) substrate assay. The total kinase activity of T204D increases linearly with increasing enzyme concentration from 100 to 400 nM ($R^2 = 0.9971$). (B) Correlation between the enzyme concentration and IC_{50} of pyrazole inhibitors, LY364947 (●) and LY566578 (◆) in the pSmad3(−3) substrate assay.

abrogated TGF-β-induced Smad2 phosphorylation in a dose-dependent manner (lanes 3−12 of parts A and B of Figure

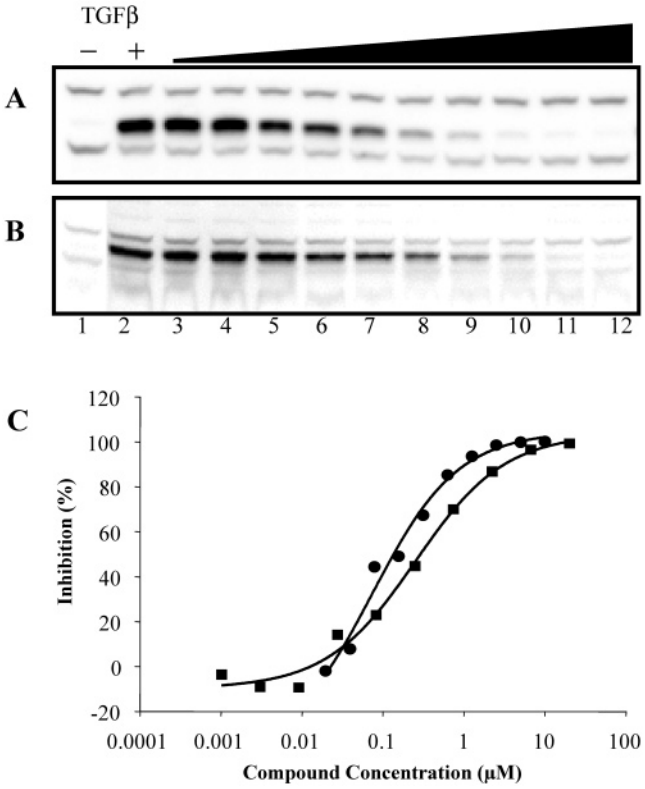

FIGURE 5: Inhibition of *in vivo* Smad2 phosphorylation by pyrazole inhibitors in NMuMg cells. Cells were treated without (lane 1) or with 100 pM TGF-β (lanes 2−12) for 2 h as described in the Experimental Procedures in the presence of a dilution series of LY364947 (A) or LY580276 (B). (C) Quantitation of *in vivo* Smad2 phosphorylation inhibition by LY364947 (●) and LY580276 (■) in NMuMg cells. The densitometric analysis was performed based upon the Western blot signals shown in A and B.

5). Quantitation of the Western blot signals demonstrated that the IC_{50} values of LY364947 and LY580276 for inhibition of *in vivo* Smad2 phosphorylation within the NMuMg cells were 135 and 290 nM, respectively (Figure 5C). These potencies correlate with the *in vitro* kinase assay IC_{50} of 58 and 175 nM, respectively. In general, cellular potency for the pyrazole series is highly correlated with the P-Smad2 inhibition assay (data not shown) and functional assays of TGF-β activity (*30*−*32*).

Consistent with previous reports of enzymatic cross-reactivity against ALK4, an activin type-I receptor, for TβRI inhibitors (*27*−*29*), the pyrazoles are capable of inhibiting activin-induced P-Smad2 and activin-responsive luciferase reporter activity in mink lung cells (data not shown). To carefully define the differential inhibition of TGF-β and BMP signaling in cells, we took advantage of the fact that NMuMg cells contain the full repertoire of TGF-β and BMP receptors and respond to both ligands. LY364947 and LY580276 reverse TGF-β-mediated growth inhibition in NMuMg cells (Figure 6A) with IC_{50} values of 0.218 ± 0.015 and 1.1 ± 0.2 μM, respectively. However, at concentrations up to 20 μM in NMuMg cells, these compounds are incapable of inhibiting BMP4-induced xVent2-luciferase activity (Figure 6B) or reversing BMP4-mediated growth inhibition (data not shown). The decrease in BMP4 response observed at 20 μM for LY364947 is likely due to the toxicity at this concentration as evidenced by the decrease in ^{3}H-thymidine incorporation in the TGF-β growth inhibition assay (Figure 6A). Interestingly, both LY364947 and LY580276 potentiate the xVent2-lux BMP4 response in NMuMg cells by ~30% ($p = 0.001$) at concentrations as low as 0.25 uM. This cellular selectivity profile within the TGF-β receptor superfamily is consistent with the homology among the type-I receptors. ALK4 and TβRI (ALK5) are highly homologous, and the BMP type-I receptors, ALK3 and ALK6, are more distantly related (*28*, *33*).

To further examine pathways outside of the TGF-β superfamily, we investigated the ability of the pyrazoles to inhibit MAPK pathways in mouse macrophage and HeLa cells. The pyrazoles are ineffective at blocking LPS-induced TNFα secretion in mouse macrophage (data not shown). LY364947 at concentrations up to 10 μM is incapable of significantly inhibiting P-p38, P-ATF2, P-MAPKAP2, and P-JNK in HeLa cells (Figure 6C). Similar results were obtained with LY566578 and other compounds from the pyrazole scaffold. Cellular pathway selectivity is further indicated by the lack of activity in combating PDGF-stimulated proliferation of NIH3T3 cells, while TGF-β−stimulated proliferation of NIH3T3 cells is potently inhibited (*30*).

Pyrazoles Block TGF-β-Induced EMT in NMuMg Cells. Given that these pyrazole compounds affect TGF-β-induced Smad2 phosphorylation in NMuMG cells, we investigated if these compounds are able to block TGF-β-mediated EMT, because this process plays important roles in the pathogenic progression of both cancer and fibrosis. Staining of the actin cytoskeleton with phalloidin revealed the characteristic epithelial architecture in control cuboidal cells with strong cortical and diffuse or punctate cytoplasmic staining (Figure 7A). Treatment with TGF-β clearly resulted in trans-differentiation from epithelial to mesenchymal morphology. Phalloidin-Alexa 488 fluorescence showed that the epithelial architecture was completely shifted to a prominent fibroblastic organization of the actin cytosketon, with distinct stress fibers (Figure 7A). Further analysis with E-cadherin, an epithelial marker, revealed that the control cells have a strong E-cadherin staining at the cytoplasmic membrane, while the cells treated with TGF-β lose this characteristic staining pattern (Figure 7A). Interestingly, when NMuMg cells were treated with pyrazole inhibitors, this EMT process was abrogated in a dose-responsive fashion. As demonstrated in parts B and C of Figure 7, 2 μM LY364947 or LY580276 prevented TGF-β-induced EMT. Lower doses partially inhibited EMT but did not completely block this transition as evidenced by the elongated morphology of the cells (E-cadherin of parts B and C of Figure 7) and actin stress fibers evident at the edges of the colonies (phalloidin of Figure parts B and C of Figure 7). This result indicates that nearly complete blockade of P-Smad activity is necessary to prevent EMT in NMuMg cells. Although LY364947 is more potent in NMuMg cells in terms of both P-Smad2 inhibition (Figure 5C) and reversing TGF-β-mediated growth inhibition (Figure 6A), it is less effective in blocking EMT at the lowest dose (0.075 μM) compared to LY580276 (parts B and C of Figure 7). The molecular details accounting for this difference require further exploration.

DISCUSSION

Alterations in the expression of TGF-β family members and their signaling pathways have been associated with

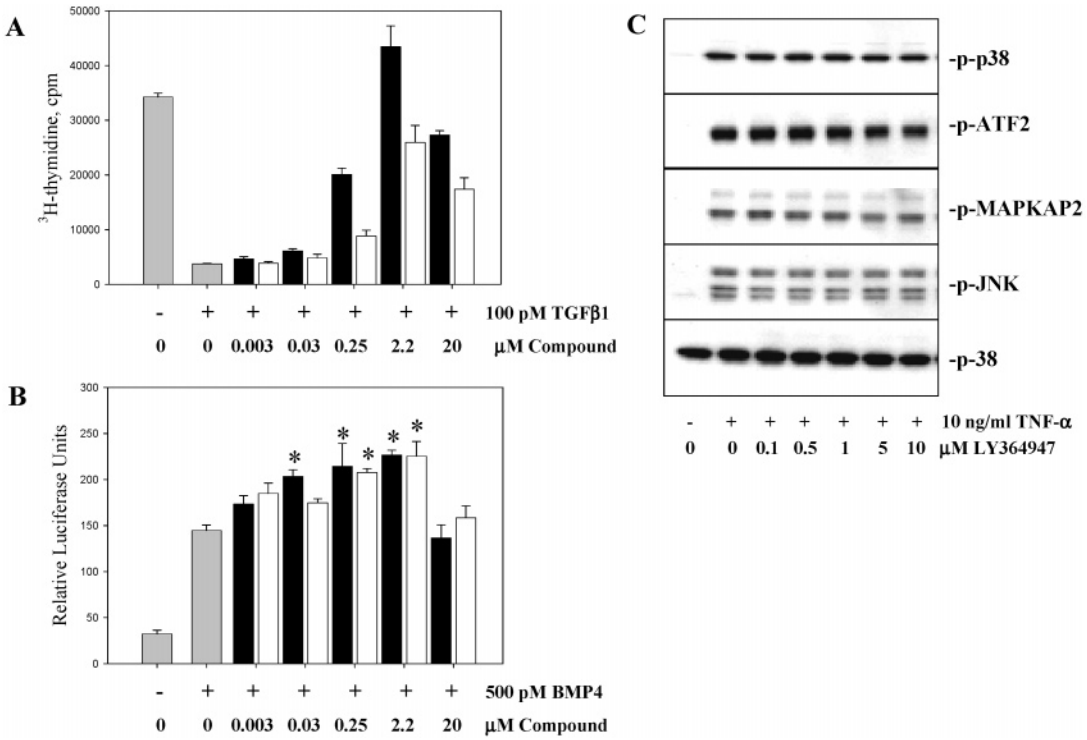

FIGURE 6: Cellular selectivity analysis of selected pyrazoles. (A) TGF-β-mediated growth inhibition is potently inhibited by LY364947 (black bars) and LY580276 (open bars). (B) NMuMg xVent2-lux cells were treated with or without 500 pM BMP4 as indicated and a dilution series of LY364947 (black bars) or LY580276 (open bars) to determine if these pyrazoles are capable of BMP pathway antagonism in cells. A statistically significant potentiation of the BMP4 response of ~30% was observed with both inhibitors. An asterisk indicates $p = 0.001$. (C) Western blot analysis of P-p38, P-ATF2, P-MAPKAPK2, P-JNK, and total p38 in HeLa cells. HeLa cells were preincubated with a dilution series of LY364947 for 30 min prior to treatment with 10 ng/mL TNFα for 15 min as indicated.

multiple human diseases including wound healing, diabetes, autoimmune diseases, fibrotic diseases, and cancer (*1*, *4*). TβRI is a major component in TGF-β-regulated signaling. The kinase domain of TβRI and its associated kinase activity are essential for TGF-β-regulated biological activity. Therefore, an effective TβRI kinase inhibitor would be anticipated to have widespread clinical applications in the treatment of cancer, fibrosis, and other human diseases. In this study, we have identified a phospho-Smad peptide, pSmad3(−3), as a substrate of TβRI kinase and established a filter-binding assay suitable for inhibitor screening and kinetic analysis of the enzyme and its inhibitors. Biochemical analysis demonstrated that pSmad3(−3) is a physiologically relevant substrate in that it is specifically phosphorylated on the C-terminal (−1 position) serine residue and is not phosphorylated by TβRII kinase. Utilizing this peptide substrate, we have demonstrated that the pyrazole TβRI kinase inhibitors are highly potent and ATP competitive inhibitors with typical tight-binding kinetics. These pyrazoles inhibit TGF-β-induced Smad2 phosphorylation within the NMuMg mammary epithelial cells with a potency equivalent to the inhibitory activity in *in vitro* kinase assays. Functional analysis revealed that these compounds are capable of blocking TGF-β-induced EMT in NMuMg cells. Cellular selectivity analysis demonstrated that pyrazoles are highly selective for the TGF-β pathway, with the notable exception of being able to potently inhibit activin signaling. Collectively, their potency in inhibiting TβRI kinase activity, favorable kinetic properties, and ability to inhibit TGF-β-induced Smad2 phosphorylation and EMT within mammary epithelial cells in conjunction with a remarkable cellular selectivity profile makes this class of pyrazoles interesting candidates for further drug development and useful tools to dissect the intricacies of TGF-β signaling.

Smad proteins lack any known structural motifs, but all members possess two highly conserved amino- and carboxyl-terminal domains (MH1 and MH2, respectively) that are separated by a nonconserved linker region. Biochemical and biological studies have clearly demonstrated that Smad proteins are essential components of serine/threonine kinase receptor signaling pathways that are regulated by phosphorylation. It has been demonstrated that Smad2 interacts transiently with and is a direct substrate of TβRI. Phosphorylation sites on Smad2 are localized to a carboxy-terminal fragment containing three serine residues at positions 464, 465, and 467. Serine 464 is not a site of phosphorylation but is important for efficient phosphorylation of Smad2. Phosphorylation at both serine 465 and 467 sites is required to mediate association of Smad2 with Smad4 in mammalian cells. Mutation of either serine 465 or 467 prevents dissociation of Smad2 from activated TβRI and blocks TGF-β-dependent signaling and Smad2 transcriptional activity (*24*, *25*). The C-terminal regions around the phosphorylation sites are highly conserved between Smad2 and Smad3. In this study, we have synthesized a set of short peptides that mimic the C-terminal sequences of Smad2 and Smad3 proteins. Phosphoserine was incorporated in the −1 or −3 position of some of the peptides. The phosphorylated peptides are better substrates of TβRI kinase *in vitro*, with the −3 position phosphoserine having the best activity in both Smad3 and Smad2 contexts. Recombinant full-length Smad2 protein that was expressed and purified from Sf9 insect cells was poorly phosphorylated by TβRI kinase *in vitro* (data not shown). This result suggests that accessory proteins (e.g., SARA) are

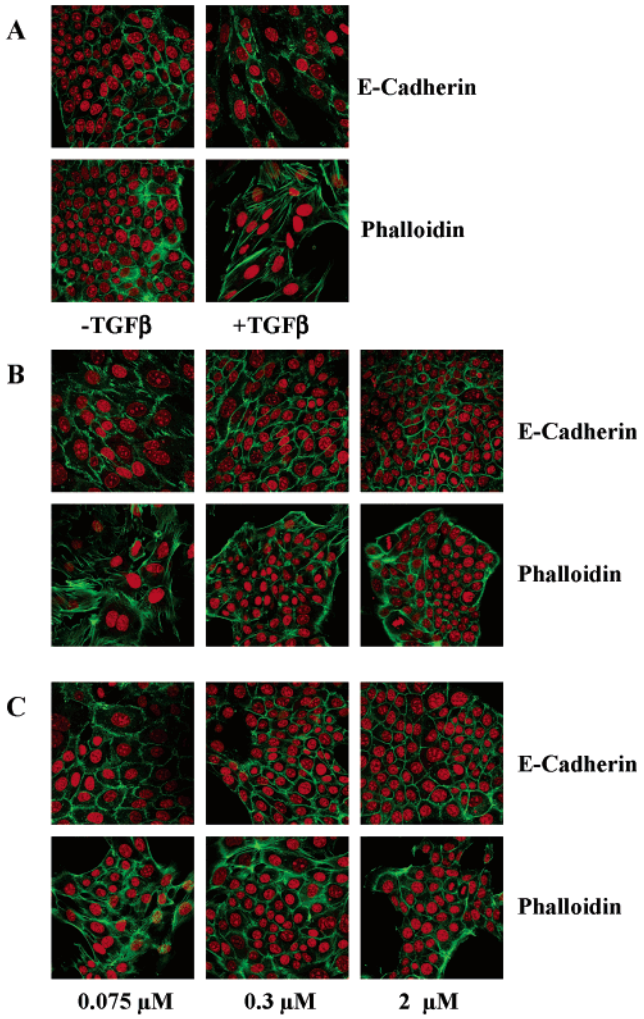

FIGURE 7: Blockade of TGF-β-induced EMT in NMuMg cells by pyrazole inhibitors. (A) Cells were treated without (left panels) or with (right panels) 100 pM TGF-β1 for 24 h and then stained with either E-cadherin antibody (upper panels) or phalloidin (lower panels) as described in the Experimental Procedures to confirm the EMT. The ability of TGF-β to induce EMT in the presence of TβRI kinase inhibitors was then examined in cells that had been treated with 100 pM TGF-β1 in the presence of 0.075, 0.3, or 2 μM LY364947 (B) or LY580276 (C) for 24 h to assess their ability to prevent TGF-β-induced EMT. All images are at 40× magnification.

integral to efficient phosphorylation of Smad proteins by TβRI kinase in cells (*34*). The phosphorylated Smad peptide provides an ideal conformation and enhanced binding affinity for efficient *in vitro* phosphorylation.

We have demonstrated that pSmad3(−3) is an effective substrate for *in vitro* phosphorylation of TβRI kinase. To demonstrate if this artificial peptide is a physiologically relevant substrate for TβRI kinase, we have performed a detailed analysis of its phosphorylated product. There is only one phosphate group added to the peptide as revealed by mass spectrum analysis, although there are multiple potential phosphorylation sites in the peptide. Mutation analysis of the peptide demonstrated that the phosphate group was transferred to the C-terminal serine residue, the physiologic phosphorylation site of the parent Smad protein within cells. Importantly, specificity analysis showed that the pSmad3(−3) peptide was phosphorylated by only TβRI kinase and not TβRII kinase, although these two kinases belong to the same family with high sequence homology in the kinase domains. Therefore, we believe that pSmad3(−3) is a specific and physiologically relevant peptide substrate for TβRI kinase and is suitable for the identification of TβRI kinase inhibitors. Compounds identified in this manner would be expected to block TGF-β-dependent biological activities.

The identification of pSmad3(−3) as a TβRI kinase substrate allows us to perform detailed kinetic analysis for the enzyme and its inhibitors. The kinetic analysis revealed that this class of compounds is ATP competitive, indicating that they are binding in the ATP-binding pocket of the TβRI kinase. This ATP competitive mechanism was further confirmed by recent cocrystallization studies in our laboratories and others (*30*, *31*, *33*, *35*). Many small molecules have been identified as potent inhibitors of serine/threonine kinases as well as tyrosine kinases (*27*−*32*, *36*, *37*). Most of these kinase inhibitors act through interaction with the ATP-binding site. Absolute specificities have not been achieved to date, which complicates their use in the treatment of diseases (*36*−*38*). However, it has been possible to develop inhibitors with a high degree of selectivity as shown above for LY364947, LY580276, and LY566578. The specificity of ATP competitive inhibitors remains a significant challenge for clinical application of kinase inhibitors. The tight-binding kinetic property of these pyrazoles and related dihydropyrrolopyrazoles (*31*, *32*) for their intended target, TβRI, may be advantageous in this regard (*39*).

The ability of the pyrazoles to specifically inhibit phosphorylation of Smad2 in NMuMg cells provides a strong foundation for further development of highly specific TβRI kinase inhibitors. Selectivity analysis against an *in vitro* serine/threonine and tyrosine kinase panel as well as cellular assays indicate that these pyrazoles are highly selective. All TβRI kinase inhibitors reported to date (*27*−*29*), including the pyrazoles described here are cross-reactive with the highly homologous ALK4 kinase giving them the ability to inhibit activin signaling. Whether this activity is a benefit or liability will have to await further preclinical and ultimately clinical investigation. The ability of these pyrazoles to potentiate BMP4 signaling in NMuMg cells is consistent with previously reported results in C2C12 cells for SB-431542 and is indicative of the therapeutic potential of TGF-β receptor kinase inhibition in terms of bone formation (*40*).

The mammary epithelial cell line, NMuMg, is a suitable model system to study EMT mediated by TGF-β (*41*, *42*). In this study, we have confirmed that TGF-β induces the EMT process in NMuMg cells and demonstrated that this process can be effectively blocked by TβRI kinase inhibitors (Figure 7). Recently, Ge and colleagues published similar results using a different TβRI kinase inhibitor, SD-093 (*43*). As previously discussed, TGF-β-induced EMT plays important roles in the progression of both cancer and chronic renal disease. In cancer, EMT generally predicts a more aggressive behavior of the tumor cells (*15*, *16*). During carcinogenesis, epithelial cells can undergo mesenchymal transformation to a fibroblast-like phenotype, thus gaining the ability to migrate, invade, and metastasize. TGF-β has been shown to play an important role in the EMT process (*17*, *41*) and in the malignant progression of fibroblast-like squamous carcinoma cells to highly invasive spindle cell carcinomas during *in vivo* skin carcinogenesis (*44*). The inhibition of autocrine TGF-β signaling in carcinoma cells reduces cell

invasiveness and tumor metastasis, and these effects of TGF-β are associated with its ability to induce EMT (*17*, *18*). In addition, myofibroblast activation is a key event in the progression of chronic renal disease. Emerging evidence suggests that myofibroblasts can be derived from tubular epithelial cells by an EMT process (*21*). TGF-β also plays a central role in tissue fibrogenesis after injury (*19*, *20*). TGF-β-induced EMT again plays an important role in the pathogenic process of chronic renal interstitial fibrosis. Therefore, TGF-β-induced EMT represents an important morphological change and physiological process involved in the pathogenesis of both cancer and fibrotic diseases. The ability of the pyrazoles reported here to effectively inhibit TGF-β-induced EMT in NMuMg cells suggests that these compounds are capable of blocking TGF-β-mediated functions *in vivo* and thus have great potential for further drug development to treat cancer, fibrosis, and potentially other human diseases.

ACKNOWLEDGMENT

The authors thank Xiang Ye for assistance with the HeLa cellular selectivity assays and Thomas W. Muir from Rockefeller University for helpful discussions on the design of Smad peptides as substrates for the TβRI kinase. After this manuscript was submitted for publication, a paper describing a similar pSmad2 peptide substrate for TβRI kinase was published by Dr. Muir and his colleagues (*45*). We also wish to thank Carl Henrick-Heldin of the Ludwig Institute for Cancer Research for providing the phospho-Smad2 (PS2) antibody and Ken Cho of the University of California−Irvine for the xVent2-luciferase construct.

REFERENCES

1. Roberts, A. B., and Sporn, M. B. (1990) The transforming growth factor-β in *Handbook of Experimental Pharmacology, Peptide, Growth Factors, and Their Receptors* (Sporn, M. B., and Roberts, A. B., Eds.) pp 419−472, Springer, Heidelberg, Germany.
2. Derynck, R., and Feng, X. H. (1997) TGF-β receptor signaling, *Biochim. Biophys. Acta 133*, F105−F150.
3. Yue, J., and Mulder, K. M. (2001) Transforming growth factor-β signal transduction in epithelial cells, *Pharmacol. Ther. 91*, 1−34.
4. Massagué, J. (1998) TGF-β signal transduction, *Annu. Rev. Biochem. 67*, 753−791.
5. Wrana, J. L., Attisano, L., Càrcamo, J., Zentella, A., Doodey, J., Laiho, M., Wang, X.-F., and Massagué, J. (1992) TGF β signals through a heteromeric protein kinase receptor complex, *Cell 71*, 1003−1014.
6. Wrana, J. L., Attisano, L., Wieser, R., Ventura, F., and Massagué, J. (1994) Mechanism of activation of the TGF-β receptor, *Nature 370*, 341−347.
7. ten Dijke, P., Yamashita, H., Ichijo, H., Franzen, P., Laiho, M., Miyazono, K., and Heldin, C. H. (1994) Characterization of type I receptors for transforming growth factor-β and activin, *Science 264*, 101−104.
8. Wrana, J. L., and Attisano, L. (1996) MAD-related proteins in TGF-β signaling, *Trends Genet. 12*, 493−496.
9. ten Dijke, P., Miyazono, K., and Heldin, C. H. (2000) Signaling inputs converge on nuclear effectors in TGF-β signaling, *Trends Biochem. Sci. 25*, 64−70.
10. Massagué, J., and Chen, Y.-G. (2000) Controlling TGF-β signaling, *Genes Dev. 14*, 627−644.
11. Derynck, R., Akhurst, R. J. and Balmain, A. (2001) TGF-β signaling in tumor suppression and cancer progression, *Nat. Genet. 29*, 117−129.
12. Siegel, P. M., and Massague, J. (2003) Cytostatic and apoptotic actions of TGF-β in homeostasis and cancer, *Nat. Rev. Cancer 3*, 807−820.
13. Hay, E. D. (1995) An overview of epithelio−mesenchymal transformation, *Acta Anat. 154*, 8−20.
14. Boyer, B., Valles, A. M., and Thiery, J. P. (1996) Model systems of epithelium−mesenchyme transitions, *Acta Anat. 156*, 227−239.
15. Gilles, C., and Thompson, E. W. (1996) The epithelial to mesenchymal transition and metastatic progression in carcinoma, *Breast J. 2*, 83−96.
16. Thiery, J. P. (2002) Epithelial−mesenchymal transitions in tumour progression, *Nat. Rev. Cancer 2*, 442−454.
17. Oft, M., Heider, K. H., and Beug, H. (1998) TGFβ signaling is necessary for carcinoma cell invasiveness and metastasis, *Curr. Biol. 8*, 1243−1252.
18. Bandyopadhyay, A., Zhu, Y., Cibull, M. L., Bao, L., Chen, C., and Sun, L. (1999) A soluble transforming growth factor β type III receptor suppresses tumorigenicity and metastasis of human breast cancer MDA-MB-231 cells, *Cancer Res. 59*, 5041−5046.
19. Massagué, J., Blain, S. W., and Lo, R. S. (2000) TGFβ signaling in growth control, cancer, and heritable disorders, *Cell 103*, 295−309.
20. Stahl, P. J., and Felsen, D. (2001) Transforming growth factor-β, basement membrane, and epithelial-mesenchymal transdifferentiation: Implications for fibrosis in kidney disease, *Am. J. Pathol. 159*, 1187−1192.
21. Yang, J., and Liu, Y. (2001) Dissection of key events in tubular epithelial to myofibroblast transition and its implications in renal interstitial fibrosis, *Am. J. Pathol. 159*, 1465−1475.
22. Chen, R. H., Moses, H. L., Maruoka, E. M., Derynck, R., and Kawabata, M. (1995) Phosphorylation-dependent interaction of the cytoplasmic domains of the type I and type II transforming growth factor-β receptors, *J. Biol. Chem. 270*, 12235−12241.
23. Franzen, P., ten Dijke, P., Ichijo, H., Yamashita, H., Schulz, P., Heldin, C. H., and Miyazono, K. (1993) Cloning of a TGF β type I receptor that forms a heteromeric complex with the TGF β type II receptor, *Cell 75*, 681−692.
24. Abdollah, S., Macias-Silva, M., Tsukazaki, T., Hayashi, L. A., and Wrana, J. L. (1997) TβRI phosphorylation of Smad2 on Ser465 and Ser467 is required for Smad2−Smad4 complex formation and signaling, *J. Biol. Chem. 272*, 27678−27685.
25. Souchelnytskyi, S., Tamaki, K., Engstrom, U., Wernstedt, C., ten Dijke, P., and Heldin, C. H. (1997) Phosphorylation of Ser465 and Ser467 in the C terminus of Smad2 mediates interaction with Smad4 and is required for transforming growth factor-β signaling, *J. Biol. Chem. 272*, 28107−28115.
26. Wieser, R., Wrana, J. L., and Massagué, J. (1995) GS domain mutations that constitutively activate TβR-I, the downstream signaling component in the TGF-β receptor complex, *EMBO J. 14*, 2199−2208.
27. Laping, N. J., Grygielko, E., Mathur, A., Butter, S., Bomberger, J., Tweed, C., Martin, W., Fornwald, J., Lehr, R., Harling, J., Gaster, L., Callahan, J. F., and Olson, B. A. (2002) Inhibition of transforming growth factor (TGF)-β1-induced extracellular matrix with a novel inhibitor of the TGF-β type I receptor kinase activity: SB-431542, *Mol. Pharmacol. 62*, 58−64.
28. Inman, G. J., Nicolas, F. J., Lallahan, J. F., Harling, J. D., Gaster, L. M., Reith, A. D., Laping, N. J., and Hill, C. S. (2002) SB-431542 is a potent and specific inhibitor of transforming growth factor-β superfamily type I activin receptor-like kinase (ALK) receptors ALK4, ALK5, and ALK7, *Mol. Pharmacol. 62*, 65−74.
29. DaCosta, B. S., Major, C., Laping, N. J., and Roberts, A. B. (2004) SB-505124 is a selective inhibitor of transforming growth factor-β type I receptors ALK4, ALK5, and ALK7, *Mol. Pharmacol. 65*, 744−752.
30. Sawyer, J. S., Anderson, B. D., Beigh, D. W., Campbell, R. M., Jones, M. L., Herron, D. K., Lampe, J. W., McCowan, J. R., McMillen, W. T., Mort, N., Parsons, S., Smith, E. C. R., Veith, M., Weir, L. C., Yan, L., and Yingling, J. M. (2003) Synthesis and activity of new aryl- and heteroaryl-substituted pyrazole inhibitors of the transforming growth factor-β type I receptor kinase domain, *J. Med. Chem. 46*, 3953−3956.
31. Sawyer, J. S., Anderson, B. D., Beight, D. W., Campbell, R. M., Goodson, T., Jr, Herron, D. K., Li, H. Y., McMillen, W. T., Mort, N., Parsons, S., Smith, E. C., Wagner, J. R., Yan, L., Zhang, F., Yingling, J. M. (2004) Synthesis and activity of new aryl- and heteroaryl-substituted 5,6-dihydro-4H-pyrrolo[1,2-β]pyrazole inhibitors of the transforming growth factor-β type I receptor kinase domain, *Bioorg. Med. Chem. Lett. 14*, 3581−3584.
32. Li, H. Y., Wang, Y., Yan, L., Campbell, R. M., Anderson, B. D., Wagner, J. R., and Yingling, J. M. (2004) Novel and potent transforming growth factor β type I receptor kinase domain

inhibitor: 7-Amino 4-(2-pyridin-2-yl-5,6-dihydro-4H-pyrrolo[1,2-β]pyrazol-3-yl)-quinolines, *Bioorg. Med. Chem. Lett. 14*, 3585−3588.
33. Singh, J., Ling, L. E., Sawyer, J. S., Lee, W. C., Zhang, F., and Yingling, J. M. (2004) Transforming the TGFβ pathway: Convergence of distinct lead generation strategies on a novel kinase pharmacophore for TβRI (ALK5), *Curr. Opin. Drug Discovery Dev. 7*, 437−445.
34. Tsukazaki, T., Chiang, T. A., Davison, A. F., Attisano, L., and Wrana, J. L. (1998) SARA, a FYVE domain protein that recruits Smad2 to the TGFβ receptor, *Cell 11*, 779−791.
35. Singh, J., Chuaqui, C. E., Boriack-Sjodin, P. A., Lee, W. C., Pontz, T., Corbley, M. J., Cheung, H. K., Arduini, R. M., Mead, J. N., Newman, M. N., Papadatos, J. L., Bowes, S., Josiah, S., and Ling, L. E. (2003) Successful shape-based virtual screening: The discovery of a potent inhibitor of the type I TGFβ receptor kinase (TβRI), *Bioorg. Med. Chem. Lett. 13*, 4355−4359.
36. Lee, J. C., and Adams, J. L. (1995) Inhibitors of serine/threonine kinases, *Curr. Opin. Biotechnol. 6*, 657−661.
37. Dancey, J., and Sausville, E. A. (2003) Issues and progress with protein kinase inhibitors for cancer treatment, *Nat. Rev. Drug Discovery 2*, 296−313.
38. Taylor, S., and Radzio-Andzelm, E. (1997) Protein kinase inhibition: Natural and synthetic variations on a theme, *Curr. Opin. Chem. Biol. 1*, 219−226.
39. Swinney, D. C. (2004) Biochemical mechanisms of drug action: What does it take for success? *Nat. Rev. Drug Discovery 3*, 801−808.
40. Shingo, M., Hayashi, M., Komiya, S., Imamura, T., and Miyazono, K. (2004) Endogenous TGF-β signaling suppresses maturation of osteoblastic mesenchymal cells, *EMBO J. 23*, 552−563.
41. Miettinen, J. P., Ebner, R., Lopez, A. R., and Derynck, R. (1994) TGF-β induced transdifferentiation of mammary epithelial cells to mesenchymal cells: Involvement of type I receptors, *J. Cell. Biol. 127*, 2021−2036.
42. Piek, E., Moustakas, A., Kurisaki, A, Heldin, C. H., and ten Dijke, P. (1999) TGF-β type I receptor/ALK-5 and Smad proteins mediate epithelial to mesenchymal transdifferentiation in NMuMG breast epithelial cells, *J. Cell Sci. 112*, 4557−4568.
43. Ge, R., Rajeev, V., Subramanian, G., Reiss, K. A., Liu, D., Higgins, L., Joly, A., Dugar, S., Chakravarty, J., Henson, M., McEnroe, G., Schreiner, G., and Reiss, M. (2004) Selective inhibitors of type I receptor kinase block cellular transforming growth factor-β signaling, *Biochem. Pharmacol. 68*, 41−50.
44. Cui, W., Fowlis, D. J., Bryson, S., Duffie, E., Ireland, H., Balmain, A. and Arhurst, R. J. (1996) TGFβ1 inhibits the formation of benign skin tumors, but enhances progression to invasive spindle carcinomas in transgenic mice, *Cell 86*, 531−542.
45. Ottesen J. J., Huse, M., Sekedat, M. D., and Muir, T. W. (2004) Semisynthesis of phosphovariants of Smad2 reveals a substrate preference of the activated TβRI kinase, *Biochemistry 43*, 5698−5706.

BI048851X